Nano Res. 2012, 5(3): 172–180
DOI 10.1007/s12274-012-0197-2
Research Article

ISSN 1998-0124
CN 11-5974/O4

# Anomalous Kink Behavior in the Current–Voltage Characteristics of Suspended Carbon Nanotubes

Moh Amer, Adam Bushmaker, and Steve Cronin (✉)

3710 McClintock Ave., Department of Electrical Engineering, University of Southern California, Los Angeles, California, 90089, USA

Received: 20 October 2011 / Revised: 27 December 2011 / Accepted: 30 December 2011


## ABSTRACT

Electrically-heated suspended, nearly defect-free, carbon nanotubes (CNTs) exhibiting negative differential conductance in the high bias regime experience a sudden drop in current (or "kink"). The bias voltage at the kink ($V_{kink}$) is found to depend strongly on gate voltage, substrate temperature, and gas environment. After subtracting the voltage drop across the contacts, however, the kink bias voltages converge around 0.2 V, independent of gate voltage and gas environment. This bias voltage of 0.2 V corresponds to the threshold energy of optical phonon emission. This phenomenon is corroborated by simultaneously monitoring the Raman spectra of these nanotubes as a function of bias voltage. At the kink bias voltage, the *G* band Raman modes experience a sudden downshift, further indicating threshold optical phonon emission. A Landauer model is used to fit these kinks in various gas environments where the kink is modeled as a change in the optical phonon lifetime, which corresponds to a change in the non-equilibrium factor that describes the existence of hot phonons in the system.

## KEYWORDS

Negative differential conductance, negative differential resistance, hot optical phonons, preferential heating, *G* band downshift

The electrical properties of carbon nanotubes (CNTs) have captured the excitement of many scientists and engineers, based on reports of ballistic electron conduction [1], negative differential resistance [2], Coulomb blockade [3], Mott insulating states [4, 5], and Luttinger liquid behavior [6]. Of particular interest is the mechanism by which electrons dissipate heat to the lattice [7]. Under high bias voltages, carbon nanotubes have demonstrated an exceptionally high current-carrying capacity, which exceeds that of the noble metals by several orders of magnitude [1, 8–10]. Electron-acoustic phonon scattering is strongly suppressed in nanotubes due to their one-dimensional band structure, which severely restricts the number of possible scattering states [11]. In the low electric field limit, electrons accelerate in the applied electric field until they gain enough kinetic energy to emit optical phonons. Consequently, optical phonons are the dominant scattering mechanism in suspended carbon nanotubes at high bias.

Yao et al. first proposed an optical phonon scattering mechanism to explain current saturation in metallic

Address correspondence to scronin@usc.edu

nanotubes at high bias voltages [12]. Single wall CNTs suspended off the substrate exhibit negative differential resistance (NDR) under high bias voltages [2, 7, 13, 14], as a result of this optical phonon emission process. Several theoretical studies have investigated the high bias transport in CNTs, further corroborating the optical phonon scattering process [15, 16]. An enhancement in the maximum operating current of these suspended devices [7] was observed by Mann et al., and was attributed to the relaxation of hot phonons. A small drop (or "kink") in the current can be seen in their *I*–*V* characteristics, however, no further explanation or description of this feature has been given.

Here, we perform simultaneous optical and electrical measurements of this anomalous kink feature, to elucidate the underlying mechanism of energy loss and to further explore the electron–phonon interactions on which it is based. A systematic study of this kink feature was performed on a total of 17 CNT samples at various gate voltages, substrate temperatures, and in different gas environments. Raman spectroscopy provides additional information about the optical phonon dynamics in this system, which also exhibits an abrupt change at these high bias voltages. The data are fitted to a Landauer model in the two regimes above and below the kink.

Samples used in this work were fabricated as follows. Trenches were patterned in $Si/SiO_2/SiN$ wafers by reactive ion etching and wet chemical etching. Pt electrodes were then deposited perpendicular to the trenches. Fe–Mo catalyst islands were patterned on top of the Pt electrodes lithographically [13]. Nanotubes were then grown by chemical vapor deposition (CVD) at 825 °C for 10 min in a mixture of ethanol, argon, and hydrogen. Each chip has 30 potential devices. Typically, 3 or 4 devices result in an individual, single wall carbon nanotube suspended between two electrodes, as shown in Fig. 1(a). Devices studied in this work were chosen by carefully examining the appearance of NDR with a peak current of ~10/*L* μA, where *L* is the length of the suspended CNT in μm [2]. Raman spectra were recorded with a Renishaw InVia spectrometer using 532 nm and 633 nm wavelength lasers, as illustrated schematically in Fig. 1.

Figure 2(a) shows the current–voltage characteristics of a metallic suspended carbon nanotube plotted together with the $G_+$ and $G_-$ band Raman shifts. A sudden drop or "kink" in the *I*–*V* curve can be seen between 0.9 and 1 V. An abrupt drop in the $G_-$ band frequency also occurs at the kink bias voltage, while the $G_+$ band remains constant. Figure 2(b) shows the detailed Raman spectra of a metallic nanotube that illustrates this type of selective downshift [14]. The sudden downshift of the $G_-$ band at the kink bias voltage indicates an abrupt change in the nanotube temperature and/or phonon populations [17]. The striking difference in behavior between the $G_+$ and $G_-$ bands indicates thermal non-equilibrium phonon populations, as reported previously [13]. Figures S-1(a) and S-1(b) in the Electronic Supplementary Material (ESM) show similar data for nanotubes exhibiting

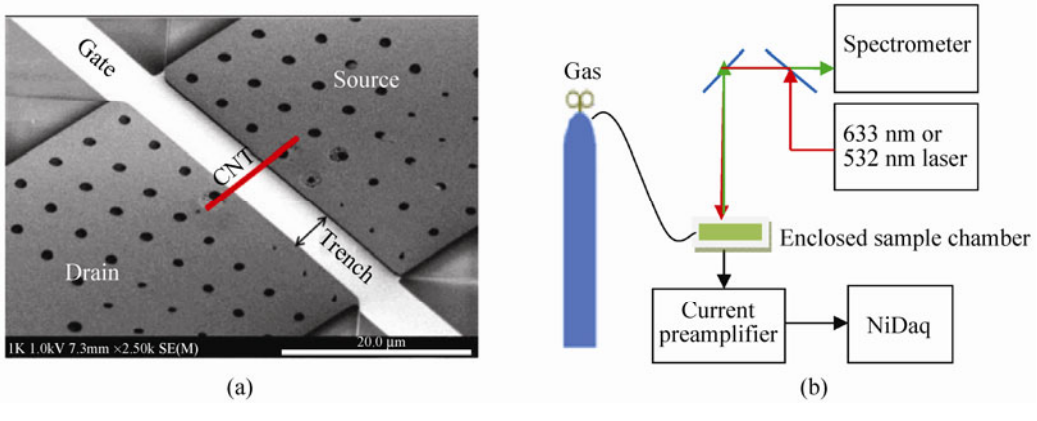


**Figure 1** (a) SEM image of a typical carbon nanotube device suspended over a trench. (b) Schematic diagram of the simultaneous electrical and optical measurement setup

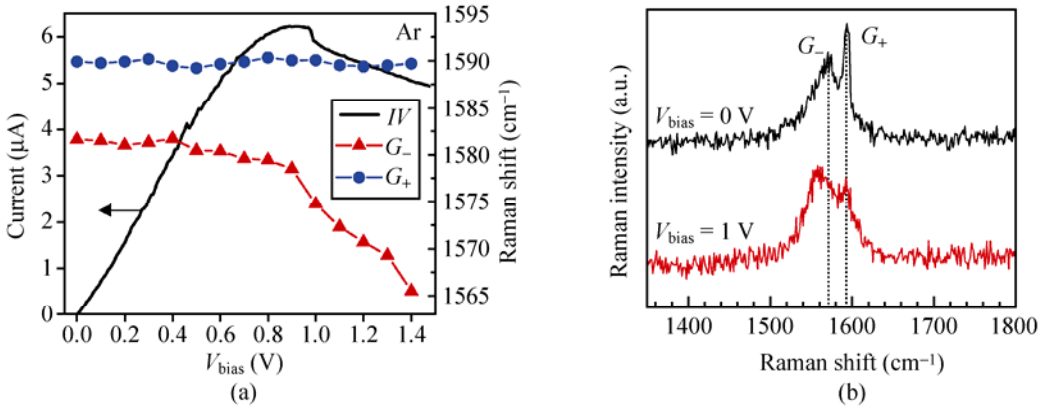


**Figure 2** (a) *I–V* characteristics and Raman data of a 2 μm metallic nanotube measured in argon at a gate voltage of –7 V plotted as a function of the applied bias voltage. (b) Raman spectra of a metallic nanotube that exhibits the downshift in (a)

preferential $G_+$ band downshifts and $G_+$ and $G_-$ downshifting together in equilibrium. Data are also shown for a semiconducting nanotube.

Figures 3(a) and 3(b) show the current–voltage characteristics of another suspended, quasi-metallic carbon nanotube measured in argon at different gate voltages between 0 and +5 V and between 0 and –5 V, respectively. A sudden drop or "kink" in the *I–V* curve can be seen in each dataset. The voltage at the kink ($V_{kink}$) varies with the applied gate voltage, as shown in Fig. 3(c). This kink bias voltage follows the same general trend as the low bias resistance of the device, also plotted in Fig. 3(c), which exhibits a maximum near zero gate voltage. The low bias resistance, which

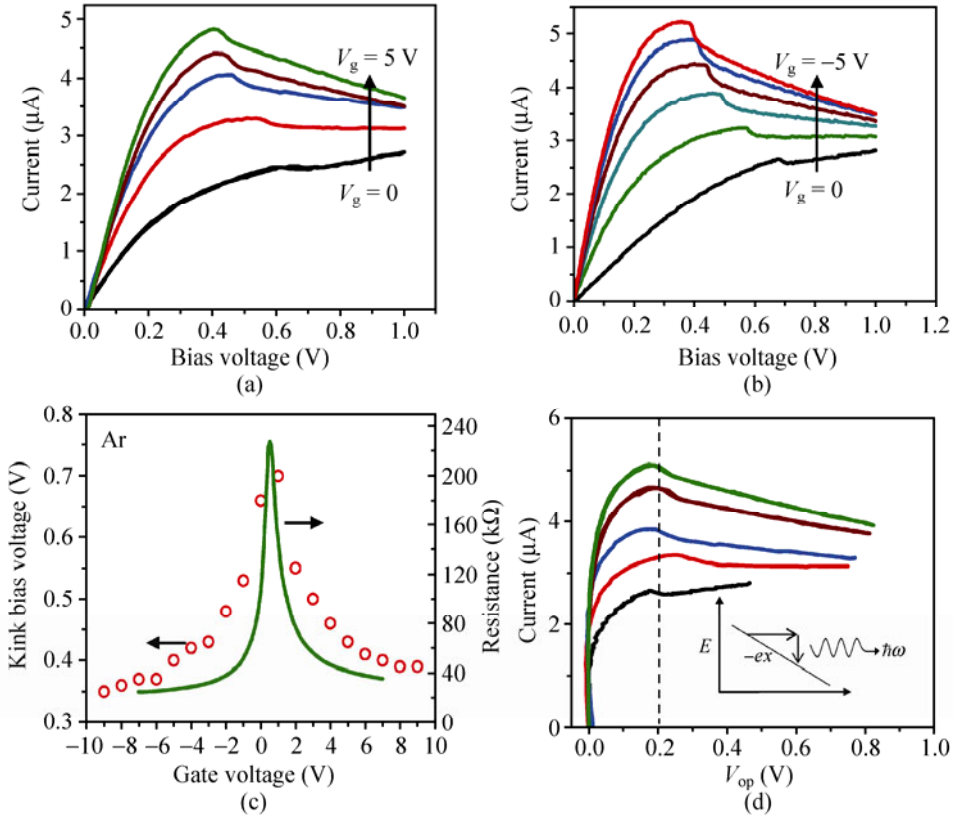


**Figure 3** (a) and (b) Current–voltage characteristics of a 2 μm nanotube measured in argon at different applied gate voltages. (c) Kink bias voltage and low bias resistance plotted as a function of the applied gate voltage. (d) Current–voltage characteristics of the nanotube in (a) plotted as a function of the voltage drop across the nanotube

is dominated by contact resistance, is modulated by the gate, which in turn shifts the kink bias voltage.

The total device resistance can be expressed as

$$R_{device} = 2R_{contact} + R_{CNT} = 2R_{contact} + R_{quantum} + R_{ac} + R_{op} \quad (1)$$

where $R_{contact}$ is the contact resistance, $R_{quantum} = h/4e^2 = 6.5\ k\Omega$ is the resistance corresponding to four units of quantum conductance $e^2/h$ associated with the spin and pseudo-spin degrees of freedom [12, 18], $R_{ac}$ is the resistance due to acoustic phonon scattering, and $R_{op}$ is the resistance associated with optical phonon scattering. $R_{contact}$ and $R_{ac}$ depend strongly on the applied gate voltage [2, 8]. In the low bias regime, $R_{op}$ is negligible since the optical phonon populations are extremely low at room temperature [2]. Therefore, the low bias resistance can be approximated as $R_{low\ bias} = 2R_{contact} + R_{quantum} + R_{ac}$. Since we are mainly interested in understanding the high bias behavior of these nanotubes, in particular the optical phonon dynamics at high bias, we can subtract the bias voltage-independent resistance as follows: $V_{op} = V_{bias} - (2IR_{contact} + IR_{quantum} + IR_{ac}) = IR_{op}$. Figure 3(d) shows the current through the nanotube plotted as a function of the voltage drop corresponding to optical phonon scattering, $V_{op}$. Here, for heavily gated and ungated $I$–$V$ curves, all the kinks occur at approximately $V_{op} = 0.2$ V, which corresponds to the energy of the highest optical phonon branches (1590 $cm^{-1}$ = 197 meV). These phonon modes are known to couple strongly to the electrons through a Kohn Anomaly [14, 15, 19]. This optical emission process is illustrated schematically in the inset of Fig. 3(d), where electrons accelerating in the applied electric field ($\varepsilon$) gain a kinetic energy that is linearly proportional to the distance they travel ($e\varepsilon x$), until they have enough energy to emit optical phonons (0.2 eV).

Figure 4(a) shows the $I$–$V$ data taken from a suspended, metallic CNT in argon and in vacuum ($1 \times 10^{-6}$ Torr). The low bias resistance of this device is not affected by the gaseous or vacuum environment. Only the high bias data is affected by the gas/vacuum environment. The corresponding Raman data are shown in Figs. 4(b) and 4(c), which plot the $G$-band Raman shift and full width half maximum (FWHM) as a function of the applied bias voltage, respectively. In Ar, there is an abrupt change in the $G$ band vibrational frequency ($\omega_G$) at the kink bias voltage, consistent with Fig. 2. In vacuum, however, the Raman data does not exhibit an abrupt change in $\omega_G$, but, instead, downshifts consistently over the whole bias voltage range. The FWHM data in Fig. 4(c) show similar results. The temperature-induced $G$ band downshifts observed in vacuum are larger than those observed in argon, because the gas molecules affect the optical phonon

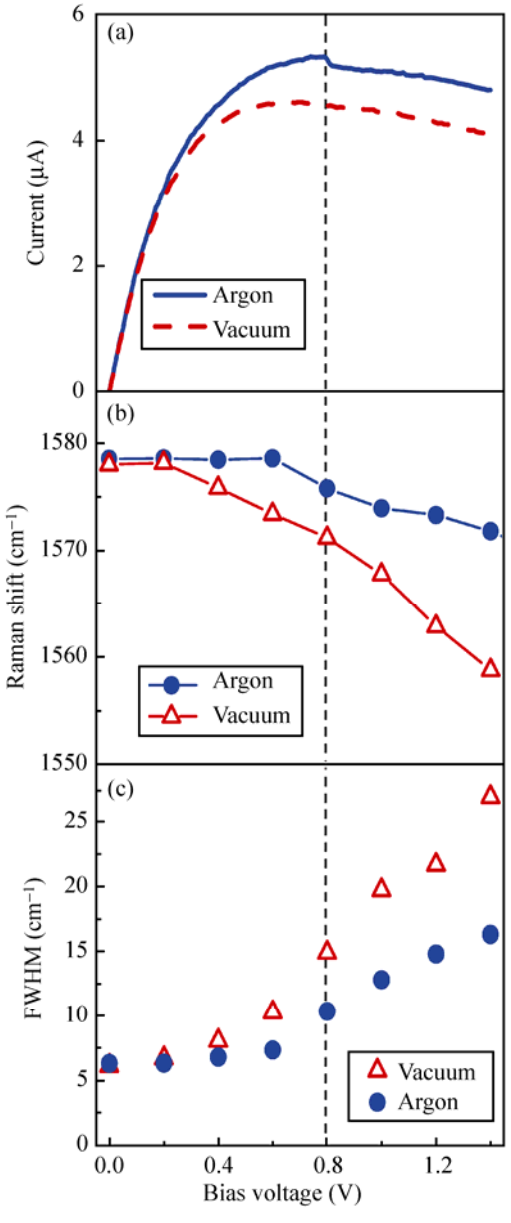


**Figure 4** (a) Current–voltage characteristics and $G$ band Raman (b) frequency and (c) linewidth for a (L~2 μm) suspended metallic nanotube measured in argon (blue circles) and vacuum (red triangles) plotted as a function of bias voltage

population, which in turns affects the thermal transport of the system [20]. At a given bias voltage, the electric current is lower in vacuum than in argon because the temperature of the nanotube is higher, and hence there is more scattering in the nanotube. The mechanism underlying this kink behavior can be understood by considering that, below the kink, gas molecules (perhaps residual gases, such as $H_2O$ and $O_2$) are adsorbed on the surface of the nanotube. These gas molecules, in turn, assist in the decay of hot optical phonons.

These hot phonons then decay rapidly into acoustic phonons, which carry the heat out of the nanotube. Above the kink, gas molecules desorb due to the population of the optical phonons, which causes a reduction in the hot phonon decay rate, causing the nanotube to heat up abruptly. That is, the desorption of gas molecules results in longer phonon lifetimes, and hence higher optical phonon (and intermediate frequency phonon) populations, which cause the abrupt downshift in the *G* band and the drop in current due to the increased electron-phonon scattering.

Figure 5(a) shows the *I*–*V* characteristics of a quasi-metallic, suspended carbon nanotube taken at various substrate temperatures between –185 and 100 ℃ in an argon environment. The kink voltage varies with base substrate temperature, as shown in the inset of Fig. 5(a). For temperatures below –130 ℃, no kink was observed in the *I*–*V* characteristics. Figure 5(b) shows the Raman shift of the $G_+$ phonon mode of the same device at various substrate temperatures, when biased at the kink. There are many temperature-dependent variables that affect the kink bias voltage, including contact resistance, thermal conductivity of the nanotube, and mean free paths. For this nanotube, these competing effects cause the kink bias voltage to peak at –40 ℃. Despite the large variations in kink bias voltage, the $G_+$ band Raman shift is observed at a consistent wavenumber (1575 $cm^{-1}$) when biased at the kink over the whole range of substrate temperatures. The $G_+$ band Raman shifts measured at zero bias voltage are plotted in the inset of Fig. 5(b), together with a polynomial fit. This data show the typical temperature dependence of the $G_+$ band mode in carbon nanotubes [17].

From the calibrated $G_+$ band downshifts, we can estimate the nanotube temperature at the kink to be approximately 400 ℃, which is consistent with the kink temperature measured for the other samples with a pronounced kink in their *I*–*V* characteristics. However, this temperature value is not accurate because of the non-equilibrium phonon populations associated with these devices [13, 14]. Figure S-2 (in the ESM) shows another set of Raman measurements taken at different substrate temperatures in He and $CO_2$ gas environments.

Figure 6(a) shows the *I*–*V* characteristics of a suspended metallic carbon nanotube measured in Ar, He, and $CO_2$ environments at a pressure of 1 atm. The kink bias voltage is highest in $CO_2$ and lowest in Ar. This trend was observed consistently on all other

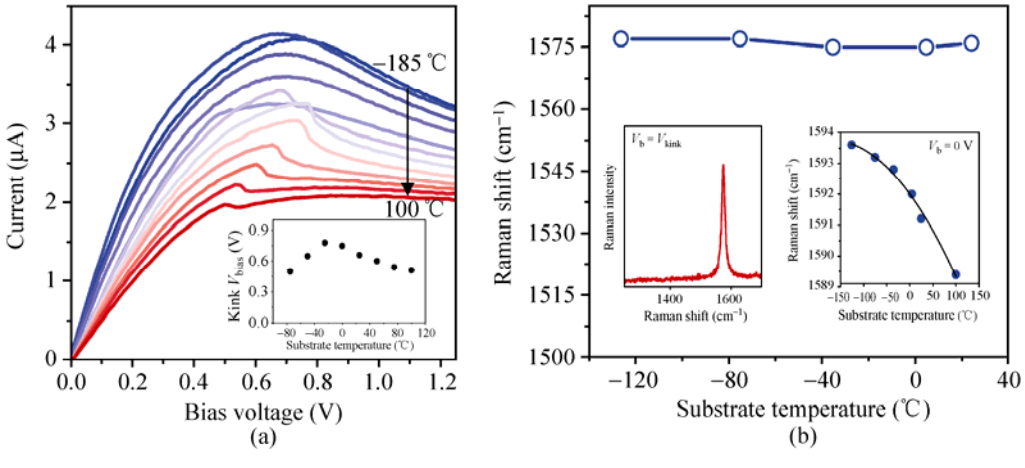


**Figure 5** (a) $I$–$V_{bias}$ data of a 5 μm suspended metallic carbon nanotube taken at different base substrate temperatures in argon. The inset shows the kink bias voltage for different substrate temperatures. (b) *G* band Raman shifts observed when the nanotube is biased at the kink at various substrate temperatures. Insets (left) Raman spectra taken at the kink and (right) zero bias *G* band Raman data with polynomial fit

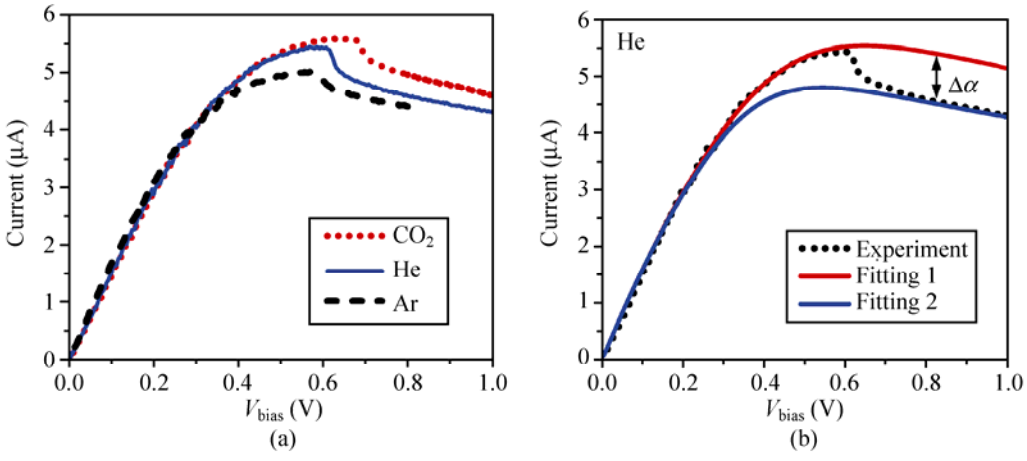


**Figure 6** (a) *I–V* characteristics of a 2 μm metallic nanotube exhibiting different kink locations for $CO_2$, He, and Ar. In (b), the dotted line shows the experimental data and the blue and red solid lines show curve fits using the model

samples measured in this study. Here, the sample was first measured in argon, then helium, and then carbon dioxide. To eliminate any irreversible effects arising from permanent changes in the nanotube structure (such as defects), the gases were pumped into the chamber several times in different orders while electrical data were recorded, to ensure the repeatability and reproducibility of these results. Before making any electrical measurements, the sample was annealed at high bias, beyond the kink, in order to remove any unwanted surface species from the previously flown gas. Figure S-3 in ESM shows additional *I–V* characteristics measured in different gas environments at various gate voltages.

This kink behavior can be modeled using a Landauer electron transport model together with a diffusive thermal transport model, coupled through the electron-phonon coupling in this system. Here, both the electron transport equations and thermal transport equations are solved self-consistently, as described previously [2, 7, 8]. The negative differential resistance observed in suspended carbon nanotubes is associated with the emission of optical phonons at high bias, which eventually decay into acoustic phonons that carry the heat out to the contacts at the ends of the nanotube. In this model, the non-equilibrium between optical and acoustic phonons is specified by a non-equilibrium factor given by

$$T_{op} = T_{ac} + a(T_{ac} - T_0) \quad (2)$$

where $T_{op}$, $T_{ac}$ and $T_0$ are the temperatures of the optical phonons, the acoustic phonons, and the substrate, respectively [2, 7, 16]. In this case, the substrate is at room temperature, giving $T_0 = 300$ K. For a constant electric power ($P$) applied to the nanotube, the spatial temperature profile assumed in the model is calculated by solving the heat diffusion equation:

$$\frac{d^2T(x)}{dx^2} + \frac{P}{A\kappa_{th}} - \frac{g(T - T_0)}{A\kappa_{th}} = 0 \quad (3)$$

where $A$, $\kappa_{th}$, and $g$, are the cross-sectional area, thermal conductivity, and heat transfer coefficient to the surrounding gas, respectively [20]. We calculate the cross-sectional area as $A = \pi d\delta$, where $d$ is the diameter of the nanotube and $\delta$ is the interlayer spacing of graphite. We also calculate the thermal conductivity of the nanotube as

$$\kappa_{th} = \frac{300\ \kappa_{th}^{300}}{T}$$

where $\kappa_{th}^{300}$ is the room temperature thermal conductivity of the nanotube [2, 21]. In Fig. 6(b), we use $\kappa_{th}^{300} = 1600$ W/(m·K) and $d = 2$ nm, based on AFM measurements [2, 22]. The non-equilibrium factor, $\alpha$, is directly proportional to the optical phonon lifetime ($\tau_{op}$) [7]. Adsorbed gas molecules enable the optical phonons to decay into lower energy phonons at a faster rate, compared with vacuum. This change in the decay rate is associated with a change in the non-equilibrium factor ($\Delta\alpha$).

The model consists of two processes describing the thermal and electrical transport. Since the two pro-

cesses are coupled through electron–phonon scattering, we must solve these iteratively, in a self-consistent fashion. The electrical conductance of our devices can be described as

$$G_{\mathrm{CNT}} = \frac{1}{R_{\mathrm{CNT}}} = \left(\frac{4e^2}{h}\right)\int_0^{\infty}\left(\frac{\lambda_{\mathrm{eff}}(E,T)}{\lambda_{\mathrm{eff}}(E,T)+L}\right)\left(\frac{\partial f}{\partial E}\right)\mathrm{d}E \quad (4)$$

where $\lambda_{\mathrm{eff}}$ is the effective mean free path of an electron, $L$ is the device length, and $\frac{\partial f}{\partial E}$ is the derivative of the Fermi–Dirac distribution [23]. The effective mean free path in the nanotube can be calculated according to Mathiessen's rule:

$$\lambda_{\mathrm{eff}}^{-1} = \lambda_{\mathrm{ac}}^{-1} + \lambda_{\mathrm{op,abs}}^{-1} + \lambda_{\mathrm{op,ems}}^{-1} \quad (5)$$

where

$$\lambda_{\mathrm{AC}}(T) = \frac{300\lambda_{\mathrm{AC}}^{300}}{T}$$

$$\lambda_{\mathrm{op,ems}} = \frac{\hbar\omega_{\mathrm{op}}L}{qV} + \lambda_{\mathrm{op,min}}\left(\frac{N_{\mathrm{op}}^{300}+1}{N_{\mathrm{op}}+1}\right)$$

and

$$\lambda_{\mathrm{op,abs}} = \lambda_{\mathrm{op,min}}\left(\frac{N_{\mathrm{op}}^{200}+1}{N_{\mathrm{op}}}\right)$$

as described previously [2, 7, 24]. In our fits, we take the room temperature mean free path for acoustic and optical phonon scattering to be $\lambda_{\mathrm{AC}}^{300}$ = 280$d$ μm and $\lambda_{\mathrm{op,min}}$ = 15$d$ nm in accordance with previously published work [23, 25]. In order to reproduce the experimental $I$–$V$ curves, Eqs. 2 and 4 are solved iteratively for each bias voltage in a self-consistent fashion until the current converges to the experimentally measured value. The values of the thermal boundary conductance of the gases used in the study were taken from Hsu et al. [20]. For the simulation results shown in Fig. 6(b), $E_{\mathrm{F}}$ is taken as 0.1 eV, which corresponds to a strongly gated quasimetallic nanotube.

Within this theoretical framework, the sudden drop in current can be explained by a change in the non-equilibrium factor ($\alpha$). Figure 6(b) shows fits of our $I$–$V$ data taken in helium above and below the kink.

Once the data below the kink were fitted to the model, $\alpha$ was varied to achieve a fit to the high bias data. That is, the only difference between fitting 1 and fitting 2 is the value of $\alpha$, which ranges from 2.5 at low bias to 4.2 at high bias. Figures S-4(a) and S-4(b) (in the ESM) show corresponding data and fits taken in argon and carbon dioxide, respectively. The extracted change in the non-equilibrium factor ($\Delta\alpha$) for argon, carbon dioxide, and helium is 0.8, 1.2, and 1.7, respectively. Table 1 shows the extracted $\Delta\alpha$ values for several other samples, determined by fitting the $I$–$V$ characteristics of each sample. From this Table, the general trend of

$$\Delta\alpha_{\mathrm{op}}^{\mathrm{Ar}} < \Delta\alpha_{\mathrm{op}}^{\mathrm{CO_2}} < \Delta\alpha_{\mathrm{op}}^{\mathrm{He}}$$

is observed for all nanotubes. The change in the non-equilibrium factor ($\Delta\alpha$), corresponds to an increase in the hot phonon decay lifetime ($\Delta\tau_{\mathrm{op}}$), which leads to increased electron–phonon scattering and a lower electrical current. This gives rise to the ordering for the change in the optical phonon decay lifetime as ($\Delta\tau_{\mathrm{op}}^{\mathrm{Ar}} < \Delta\tau_{\mathrm{op}}^{\mathrm{CO_2}} < \Delta\tau_{\mathrm{op}}^{\mathrm{He}}$), which is the same ordering measured for the ordering $\Delta I$ of the gases in Table 1. We notice that neither the change in the optical phonon decay rate nor the kink bias voltage correlate with the molecular mass of these gases or the number of atoms in these molecules, but is most likely related to the degree to which they couple vibronically to the phonons in the nanotube, which has not been studied previously.

**Table 1** Change in the electrical current ($\Delta I$) observed at the kink in Ar, He, and $CO_2$

| Samples | Type | $\Delta I_{\mathrm{Ar}}$ (μA) | $\Delta I_{\mathrm{CO_2}}$ (μA) | $\Delta I_{\mathrm{He}}$ (μA) | $\Delta\alpha_{\mathrm{Ar}}$ | $\Delta\alpha_{\mathrm{CO_2}}$ | $\Delta\alpha_{\mathrm{He}}$ |
|---|---|---|---|---|---|---|---|
| Sample 1 $L$=5 μm | M | 0.31 | N/A | N/A | 2 | N/A | N/A |
| Sample 2 $L$=2 μm | M | 0.26 | 0.48 | 0.6 | 0.55 | 0.7 | 1.2 |
| Sample 3 $L$=2 μm | SC | 0.16 | 0.2 | 0.26 | 0.3 | 0.6 | 1 |
| Sample 4 $L$=2 μm | M | 0.25 | 0.55 | 0.6 | 0.4 | 0.55 | 1.3 |
| Sample 5 $L$=2 μm | M | 0.25 | N/A | N/A | 0.5 | N/A | N/A |
| Sample 6 $L$=5 μm | SC | N/A | 0.2 | 0.25 | N/A | 1 | 1.1 |
| Sample 7 $L$=2 μm | M | 0.23 | N/A | N/A | 0.35 | N/A | N/A |
| Sample 8 $L$=2 μm | SC | 0.12 | N/A | N/A | 0.5 | N/A | N/A |

In summary, we have quantified several aspects of the sudden drop or "kink" in current observed in the *I–V* characteristics of individual, suspended carbon nanotubes in gaseous environments.

After subtracting the voltage drop across the contact resistances, the *I–V* characteristics of the carbon nanotube reveal that the kink occurs at 0.2 V independent of the gas environment and/or the gate voltage applied. This kink voltage corresponds to the energy of the optical phonon emission threshold. Raman measurements reveal a sudden downshift in the *G* band mode, indicating a sudden increase in the non-equilibrium phonon population. A strong substrate temperature dependence and gate voltage dependence of the kink bias voltage are observed. However, the Raman shift at the kink is constant over the measured range of substrate temperatures, which suggests a constant *G* band temperature. Using the Landauer formalism, the kink can be modeled as a change in the non-equilibrium optical phonon population, which increases dramatically after the kink.

## Acknowledgements

This research was supported in part by Office of Naval Research (ONR) Award No. N000141010511, Department of Energy (DOE) Award No. DE-FG02-07ER46376, and National Science Foundation (NSF) Award No. CBET-0854118. A portion of this work was done in the University of California Santa Barbara (UCSB) nanofabrication facility, part of the NSF funded National Nanotechnology Infrastructure Network (NNIN) network.

**Electronic Supplementary Material**: Supplementary material (more *I–V* and Raman data for selective downshifts, kink behavior in different gases and different substrate temperatures, and *I–V* data fits for carbon dioxide and argon) is available in the online version of this article at http://dx.doi.org/10.1007/s12274-012-0197-2.

## References

[1] Javey, A.; Guo, J.; Paulsson, M.; Wang, Q.; Mann, D.; Lundstrom, M.; Dai, H. J. High-field quasiballistic transport in short carbon nanotubes. *Phys. Rev. Lett.* **2004**, *92*, 106804.

[2] Pop, E.; Mann, D.; Cao, J.; Wang, Q.; Goodson, K.; Dai, H. J. Negative differential conductance and hot phonons in suspended nanotube molecular wires. *Phys. Rev. Lett.* **2005**, *95*, 155505.

[3] Cobden, D. H.; Bockrath, M.; McEuen, P. L.; Rinzler, A. G.; Smalley, R. E. Spin splitting and even-odd effects in carbon nanotubes. *Phys. Rev. Lett.* **1998**, *81*, 681–684.

[4] Deshpande, V. V.; Chandra, B.; Caldwell, R.; Novikov, D. S.; Hone, J.; Bockrath, M. Mott Insulating state in ultraclean carbon nanotubes *Science* **2009**, *323*, 106–110.

[5] Bushmaker, A. W.; Deshpande, V. V.; Hsieh, S.; Bockrath, M. W.; Cronin, S. B. Large modulations in the intensity of raman-scattered light from pristine carbon nanotubes. *Phys. Rev. Lett.* **2009**, *103*, 067401.

[6] Bockrath, M.; Cobden, D. H.; Lu, J.; Rinzler, A. G.; Smalley, R. E.; Balents, L.; McEuen, P. L. Luttinger-liquid behaviour in carbon nanotubes. *Nature* **1999**, *397*, 598–601.

[7] Mann, D.; Pop, E.; Cao, J.; Wang, Q.; Goodson, K.; Dai, H. J. Thermally and molecularly stimulated relaxation of hot phonons in suspended carbon nanotubes. *J. Phys. Chem.* **2006**, *110*, 1502–1505.

[8] Park, J. Y.; Rosenblatt, S.; Yaish, Y.; Sazonova, V.; Üstünel, H.; Braig, S.; Arias, T. A.; Brouwer, P. W.; McEuen P. L. Electron-phonon scattering in metallic single-walled carbon nanotubes. *Nano Lett.* **2004**, *4*, 517–520.

[9] McEuen, P. L.; Fuhrer, M. S.; Park, H. K. Single-walled carbon nanotube electronics. *IEEE Trans. Nanotechnol.* **2002**, *1*, 78–85.

[10] Radosavljevic, M.; Lefebvre, J.; Johnson, A. T. High-field electrical transport and breakdown in bundles of single-wall carbon nanotubes. *Phys. Rev. B* **2001**, *64*, 241307.

[11] Giamarchi, T. *Quantum physics in one dimension*; Oxford University Press: USA, 2004.

[12] Yao, Z.; Kane, C. L.; Dekker, C. High-field electrical transport in single-wall carbon nanotubes. *Phys. Rev. Lett.* **2000**, *84*, 2941–2944.

[13] Bushmaker, A. W.; Deshpande, V. V.; Hsieh, S.; Bockrath, M. W.; Cronin, S. B. Gate voltage controllable non-equilibrium and non-ohmic behavior in suspended carbon nanotubes. *Nano Lett.* **2009**, *9*, 2862–2866.

[14] Bushmaker, A. W.; Deshpande, V. V.; Bockrath, M. W.; Cronin, S. B. Direct observation of mode selective electron-phonon coupling in suspended carbon nanotubes. *Nano Lett.* **2007**, *7*, 3618–3622.

[15] Piscanec, S.; Lazzeri, M.; Robertson, J.; Ferrari, A. C.; Mauri, F. Optical phonons in carbon nanotubes: Kohn anomalies, Peierls distortions, and dynamic effects. *Phys. Rev. B* **2007**, *75*, 035427.

[16] Lazzeri, M.; Piscanec, S.; Mauri, F.; Ferrari, A. C.; Robertson, J. Electron transport and hot phonons in carbon nanotubes. *Phys. Rev. Lett.* **2005**, *95*, 236802.

[17] Bonini, N.; Lazzeri, M.; Marzari, N.; Mauri, F. Phonon anharmonicities in graphite and graphene. *Phys. Rev. Lett.* **2007**, *99*, 176802.

[18] Supriyo, D. *Electronic transport in mesoscopic systems*; Cambridge University Press: Cambridge and New York, 1997.

[19] Farhat, H.; Son, H.; Samsonidze, G. G.; Reich, S.; Dresselhaus, M. S.; Kong, J. Phonon softening in individual metallic carbon nanotubes due to the Kohn anomaly. *Phys. Rev. Lett.* **2007**, *99*, 145506.

[20] Hsu, I. K.; Pettes, M. T.; Aykol, M.; Shi, L.; Cronin, S. B. The effect of gas environment on electrical heating in suspended carbon nanotubes. *J. Appl. Phys*. **2010**, *108*, 084307.

[21] Mingo, N.; Broido, D. A. Length dependence of carbon nanotube thermal conductivity and the "problem of long waves". *Nano Lett.* **2005**, *5*, 1221–1225.

[22] Liu, Z. W.; Bushmaker, A.; Aykol, M.; Cronin, S. B. Thermal emission spectra from individual suspended carbon nanotubes. *ACS Nano* **2011**, *5,* 4634–4640.

[23] Zhao, Y.; Liao, A.; Pop, E. Multiband mobility in semiconducting carbon nanotubes. *IEEE Electron Device Lett.* **2009**, *30*, 1078–1080.

[24] Xia, M. G.; Zhang, L.; Zhang, S. L. Effect of optical phonons scattering on electronic current in metallic carbon nanotubes. *Phys. Lett. A* **2009**, *373*, 385–390.

[25] Liao, A.; Zhao, Y.; Pop, E. Avalanche-induced current enhancement in semiconducting carbon nanotubes. *Phys. Rev. Lett.* **2008**, *101*, 256804.